MOLECULAR DYNAMICS SIMULATION OF MIXED DISLOCATION INTERACTION WITH STACKING FAULT TETRAHEDRON—H.-J. Lee and B. D. Wirth (University of California, Berkeley)

OBJECTIVE

The objective of this work is to understand the interaction mechanisms between a mixed dislocation and a commonly observed irradiation defect in face center cubic (FCC) materials, which is a stacking fault tetrahedron (SFT), with an ultimate aim of gaining insights into clear channel formation in irradiated materials.

SUMMARY

The interaction between a 60 degree mixed dislocation and a stacking fault tetrahedron (SFT) is investigated using molecular dynamics (MD) simulation. The interaction strongly depends on the sense of the dislocation Burgers vector, with un-faulting and stable shear ledge formation occurring in one case, while simple bypass and immediate reconstruction of the SFT is observed for the opposite Burgers vector direction. SFT un-faulting by a mixed dislocation occurs following the constriction of a mixed dislocation on the SFT, which produces a Shockley partial that can glide on the SFT face(s). In particular, when the dislocation intersects the SFT edge side, the SFT base is absorbed into the dislocation core as a super-jog pair. After dislocation bypass, a smaller SFT and vacancy clusters remain behind. When the dislocation glides on the base plane of the SFT, the strong repulsion between the mixed dislocation and the SFT induced SFT collapse.

PROGRESS AND STATUS

Introduction

An extensive research effort has investigated the interaction between dislocations and radiation induced defects (RIDs) to provide a theoretical framework to understand, and ultimately predict, the changes of mechanical properties of structural materials due to high-energy particle irradiation [1-3]. In face centered cubic (FCC) Copper (Cu), about 90% of the radiation defects observed in the transmission electron microscope (TEM) are stacking fault tetrahedra (SFTs) [4]. The SFTs act as obstacles to dislocation motion, thus changing the local deformation behavior of the materials, which are observed in tensile tests as increases in yield and ultimate tensile stress and decreases in the uniform ductility [5]. A common feature of the microstructure of irradiated and deformed materials (including Cu) observed by TEM is the formation of defect free channels, in which the as-irradiated defect has been removed in a localized region by the dislocation motion [6]. Such localized deformation is believed to be related to the ductility loss in irradiated materials. The micro-structural characterization of defect free channels, including their approximate width (~ 200 nm) and spacing (~ 1 μm), and the conditions of strain rate, temperature and irradiation dose (RID density) necessary for the defect free channel formation are relatively well established by TEM experiments [6]. However, the atomistic interactions between a dislocation and an SFT, and in particular a mechanism for the complete removal of an SFT, that leads to the defect free channel formation remain an open question.

Molecular dynamics (MD) simulations have been widely used to understand the atomistic interactions of edge and screw dislocations with an SFT [7-14]. When intersected by an edge dislocation, the SFT is often sheared, but absorption of the SFT base also occurs when the extra-half plane of an edge dislocation is oriented toward the base of the SFT [12]. When intersected by a screw dislocation, the SFT can either be partially absorbed or simply sheared, depending on the interaction geometry, the applied shear stress and temperature [11-14]. Thus, the resulting SFT structure consists of either a perfect SFT or two SFTs, or an SFT with defects such as ledges, vacancy clusters, or truncated base. A notable feature is that the screw dislocation spontaneously cross-slips on the SFT face and can thus partially un-fault the SFT upon intersection. Early and more recent in-situ TEM observations show that screw dislocations are more efficient than edge dislocations at removing radiation induced defects [15-18]. In particular, Matsukawa et al. reported collapse of an SFT into a smaller SFT and the annihilation of the base portion in a quenched gold by a moving screw dislocation [18].

Regarding the interaction between an SFT and a mixed dislocation, there are no known available MD simulations results, but SFT collapse into a Frank loop has been proposed by Kimura and Maddin [19]. More recently Robertson et al have observed destruction of an SFT in quenched gold by a mixed dislocation, although the mechanism has not been fully established [20].

In this report, we present the results of MD simulations of a 60 degree mixed dislocation intersecting an SFT to elucidate the interaction mechanisms. The results presented here investigate four possible interaction geometries between a mixed dislocation and an SFT, as shown in Figure 1. We found that the interaction results strongly depend on the dislocation Burgers vector direction, in which one type (b=CA) leads to partial un-faulting of the SFT and shear ledge formation while the other type (b=AC) involves simple bypass and immediate reconstruction of the SFT. For the dislocation b=CA intersecting an SFT, where the un-faulting of the SFT occurs, we found that the mixed dislocation dissociates to two Shockley partial and a stair-rod partial dislocations upon constriction on the SFT. One particular case that shows absorption of the SFT base and super-jog formation is discussed in detail and the corresponding dislocation reaction mechanism is analyzed. However, the predicted collapse mechanism by Kimura and Maddin was not observed.

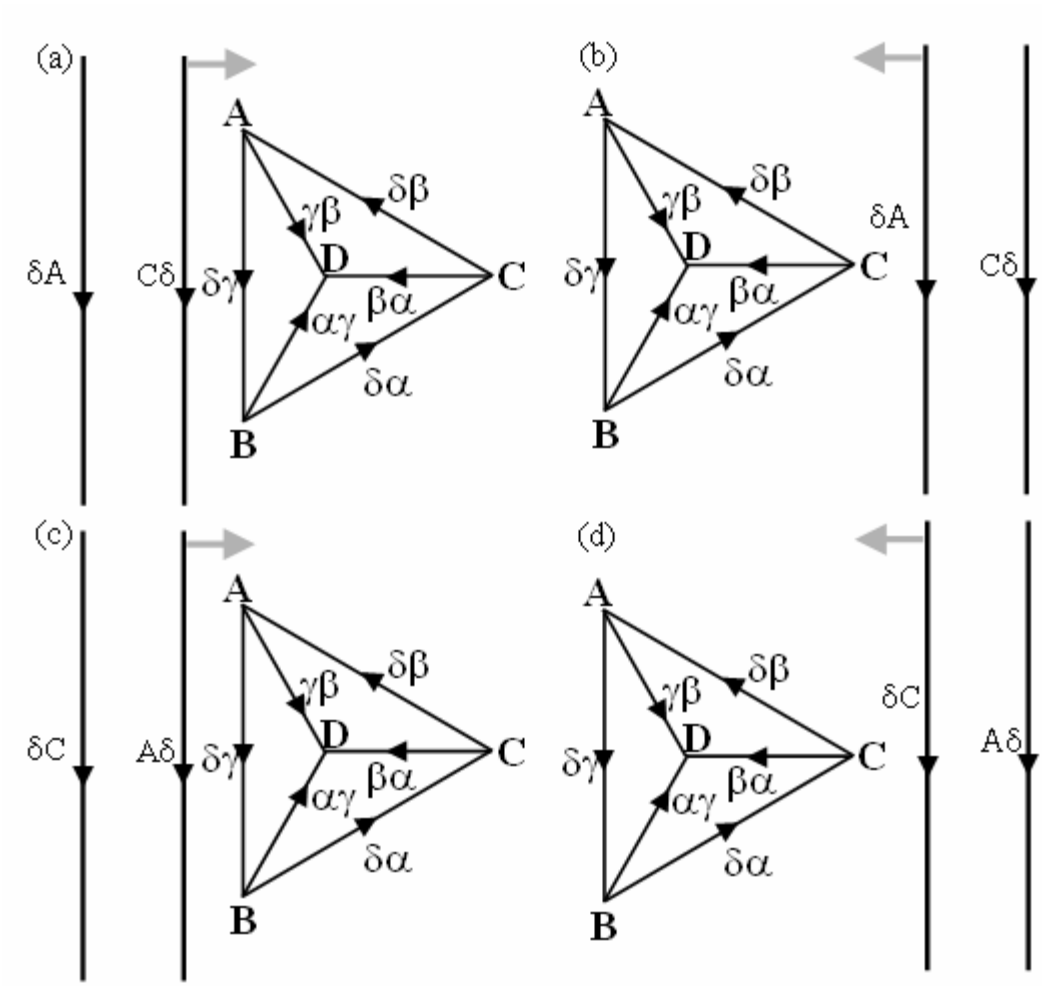

Figure 1. Schematic representation of the four possible interaction geometries between a mixed dislocation and an SFT: (a) b=CA and SFT face (b) b=CA and SFT edge (c) b=AC and SFT face (d) b=AC and SFT edge. The grey arrow indicates the dislocation gliding direction.

Simulation Methods

The MDCASK code [21] with an embedded atom method (EAM) potential by Mishin et al [22] was used to simulate an atomistic process in face centered cubic (FCC) Cu. A simulation cell with FCC crystalline structure and orientations of x=$[\bar{1}11]$, y=1/2[110] and z=1/2$[1\bar{1}2]$ is used. The size of the system used in this work is 31.4 nm in x, 22.5 nm in y, 44.3 nm in z direction, which is (50x88x100) in unit cells and contains 2,640,000 atoms. To generate an SFT, a triangular vacancy platelet of 153 vacancies is inserted in the system, which corresponds to an SFT edge length of 4.6 nm. The mixed dislocation with

b=CA is generated by introducing an edge dislocation core of b=-1/4$[1\bar{1}2]$ and screw dislocation core of b=-1/4[110] at the same location. The dislocation reaction between these two dislocations produces a perfect mixed dislocation of b=1/2$[0\bar{1}1]$ by $-1/4[110]+1/4[1\bar{1}2]\rightarrow 1/2[0\bar{1}1]$. The mixed dislocation with an opposite Burgers vector (b=AC) is generated by inserting an opposite sign of screw and edge dislocation cores at the same location.

Periodic boundary conditions are used in the y and z directions, while the x direction is a free surface, subject to an applied shear surface force. The periodic boundary condition in the z direction is modified by shifting atomic positions in the y direction to ensure the continuity of the [110] plane across the periodic boundary in the z direction, as performed in the work of Rodney [23]. To reduce the distortion of the elastic field due to the modified periodic boundary condition, we used a longer simulation cell length in the z direction (44.3 nm) compared to the x direction (31.4 nm).

The simulation cell was equilibrated for 10 ps at T = 100 K using a micro-canonical (NVE) ensemble. Following equilibration, a constant shear stress of 100 MPa is applied to the system by adding constant forces in the Burgers vector direction to the atoms on the free x surface. When the direction of the applied shear stress is reversed, the dislocation glides in the opposite direction as shown in Fig. 1(a) vs. (b) and Fig. 1(c) vs. (d).

The defect and dislocations were identified by the common neighbor method [24]. In the figures, the light colored (yellow) atoms are atoms in HCP structure, thus corresponding to stacking faults, and the dark colored (blue) atoms are neither FCC nor HCP, corresponding to a Shockley partial dislocation, a stair-rod partial dislocation, or other defect structures.

Results

Mixed dislocation (b=CA) intersecting SFT face

When the mixed dislocation glides toward the ABD face of the SFT at an applied shear stress of 100MPa, the two Shockley partials, Cδ and δA, first constrict on the SFT face as shown in Fig. 2(a). Then, a stair-rod dislocation ($\delta\gamma$) is formed at the constriction line as shown in Fig. 2(b). The Cδ leading partial continues to glide by cutting through the SFT, while the δA partial cross-slips to become γA that glides on the (c)-plane. Thus, the dislocation reaction is: Cδ+δA$\rightarrow$Cδ+$\delta\gamma$+γA. The γA reacts with the AB and AC edge of the SFT as shown in Fig. 2(b). The leading partial Cδ detaches from the SFT by cutting through the SFT and detaching around the CD edge of the SFT, while the trailing partial δA detaches from the SFT by an Orowan mechanism (Fig. 2(b)-(d)). Immediately after the detachment of both partials, the remaining structure consists of a smaller SFT and a truncated base, which is identical to the previously reported structure of a screw dislocation intersecting an SFT face [14]. Subsequently, the remaining Shockley partial δA on the BCD face of the SFT (Fig. 2(d)) moves back to the smaller SFT and the truncated base. This initiates a series of dislocation reactions that produce an SFT with shear ledges as shown in Fig. 2(e). Again, the reactions for the shear ledge formation are similar to those observed and analyzed when a screw dislocation intersects an SFT face [14]. The ledge on the ABD face is vacancy type (V) and the ledge on BCD face is interstitial type (I). Initially the I-ledge was connected to the V-ledge and parallel to the BC edge of the SFT but about half of it changes its orientation parallel to DB edge of the SFT as shown in Fig. 2(e). The detailed step-by-step dislocation analysis of this interaction and the comparison to the corresponding interaction between an SFT and screw or edge dislocation are previously reported by Lee et al. [25].

Mixed dislocation (b=CA) intersecting SFT edge

When the mixed dislocation glides toward the CD edge of the SFT, the constriction of two Shockley partials (δA and Cδ) occurs in the short segment around the CD edge. The following two reactions are observed simultaneously on the SFT faces near the constriction line around the CD edge.

$\delta A + C\delta \rightarrow \delta A + C\beta + \beta\delta$ on the ACD face ((b)-plane) of the SFT

$\delta A + C\delta \rightarrow \delta A + C\alpha + \alpha\delta$ on the BCD face ((a)-plane) of the SFT

Then, the leading partial δA glides forward by cutting through the SFT cross section while the Cβ and Cα Shockley partials glide on the ACD and BCD face of the SFT, respectively, toward the base and un-fault the SFT. When the Cβ and Cα Shockley partials reach the base of the SFT, they form the Cδ Shockley partial via reaction with the stair-rod partials at the SFT edges. The Cδ glides on and un-faults the ABC face ((d)-plane) of the SFT, which removes the C apex of the SFT as shown Fig. 3(b).

As the dislocation glides further to bypass the SFT, a super-jog appears near the A apex (Fig. 3(c)). The leading partial detaches from the SFT as the two arms of the dislocation bow and recombine around the super-jog, which then is pushed back to the SFT (Fig. 3(d)). As the trailing partial detaches from the SFT, the shear ledges starts to form (Fig. 3(e)). The I-ledge is formed on the ABD face and the V-ledge is formed on BCD face of the SFT as shown in Fig. 3(f). The shear ledges remain stable and no further reaction is observed until the second dislocation bypass. The second bypass reaction is essentially identical to the results shown in Figure 3, except that the SFT is now sheared by 2 Burgers vectors.

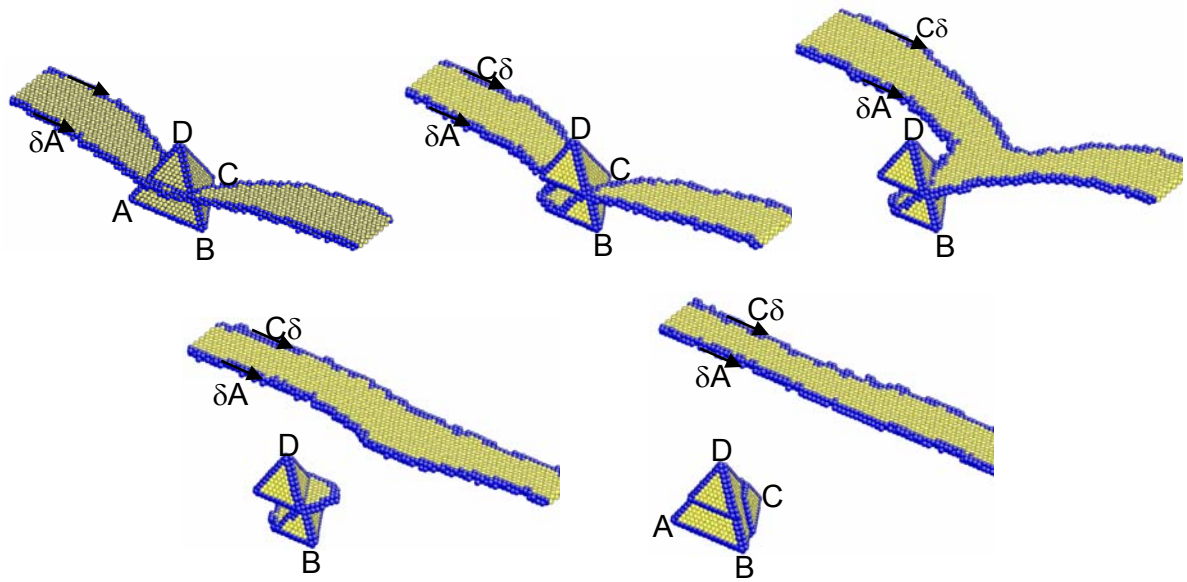

Figure 2. MD snapshots of the mixed dislocation, b=CA, intersecting SFT face:

(a) Constriction on the SFT face (32ps)
(b) Un-faulting of the c-plane (35ps)
(c) Leading partial leaves the SFT by recombining around the SFT (41ps)
(d) Trailing partial leaves the SFT by an Orowan mechanism, leaving a smaller SFT and a truncated base (59ps)
(e) Smaller SFT and the truncated base forms a sheared SFT (64ps)

Mixed dislocation (b=AC) intersecting SFT face

While the leading partial (Aδ) is pinned by the SFT, the trailing partial (δC) does not glide to constrict with the leading partial but remains at a stand-off distance of about 2.2 nm from the SFT, and begins to bow. Note that this is a considerably different interaction from the dislocation of b=CA case, where the leading and the trailing partial constrict upon the SFT face (Section 3.1). The leading partial Aδ continues to glide forward and detaches from the SFT by cutting through the SFT (Fig. 4(a)), which leaves dislocation segments on the SFT faces. Then, the trailing partial (δC) glides towards the SFT. It combines with the dislocation segments on the SFT faces and forms I- and V-ledges on the ABD and BCD face of the SFT, respectively. The shear ledges glide towards the D apex of the SFT as the trailing partial cuts through and detaches from the SFT (Fig. 4(b)-(c)). Immediately after the mixed dislocation (b=AC) bypasses, the SFT is fully reconstructed to a perfect SFT.

Mixed dislocation (b=AC) intersecting SFT edge

The leading partial (δC) intersects the CD edge of the SFT and bends around the SFT initially (Fig. 5(a)). As the trailing partial (Aδ) approaches, the leading partial cuts through the SFT and the trailing partial follows (Fig. 5(b)-(d)). During the bypass, shear ledges form on the BCD and ABD faces of the SFT. Both shear ledges move almost simultaneously toward the D apex of the SFT as the two partial dislocations detach by a shear mechanism. As in the case of the mixed dislocation of b=AC intersecting the SFT face, the SFT is fully reconstructed to a perfect SFT immediately after dislocation (b=AC) bypass.

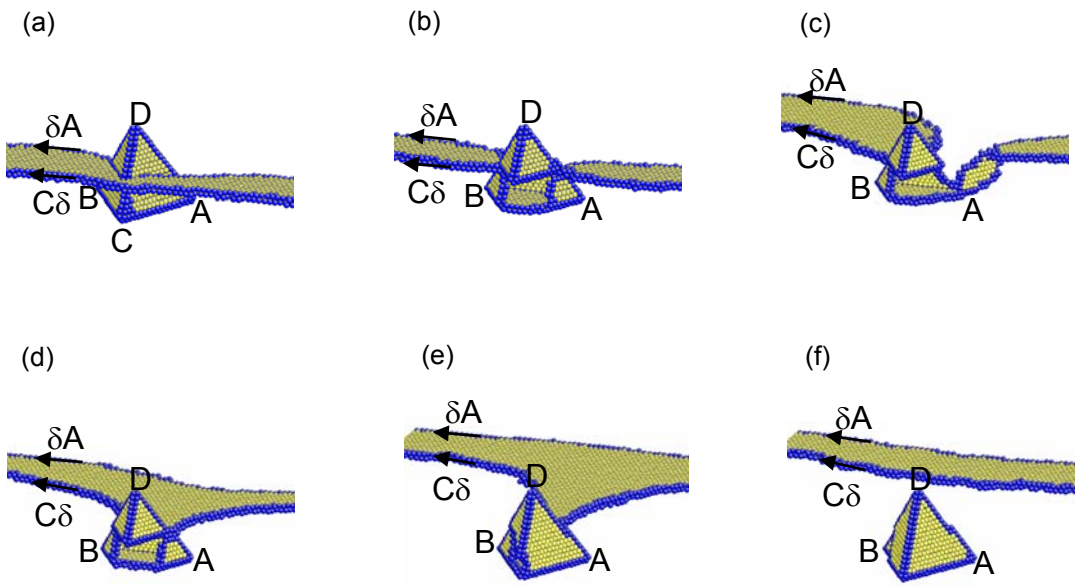

Figure 3. Interaction results of the mixed dislocation, b=CA, intersecting SFT edge:

(a) Constriction on the SFT edge (36ps)
(b) Un-faulting of the a and b-plane (38ps)
(c) Un-faulting of the c-plane (47ps)
(d) Recombination and detachment of the leading partial (50ps)
(e) Reaction between the smaller top SFT and the truncated base during the detachment of the trailing partial (67ps)
(f) Formation of an SFT with shear ledges on a and c-plane (70ps)

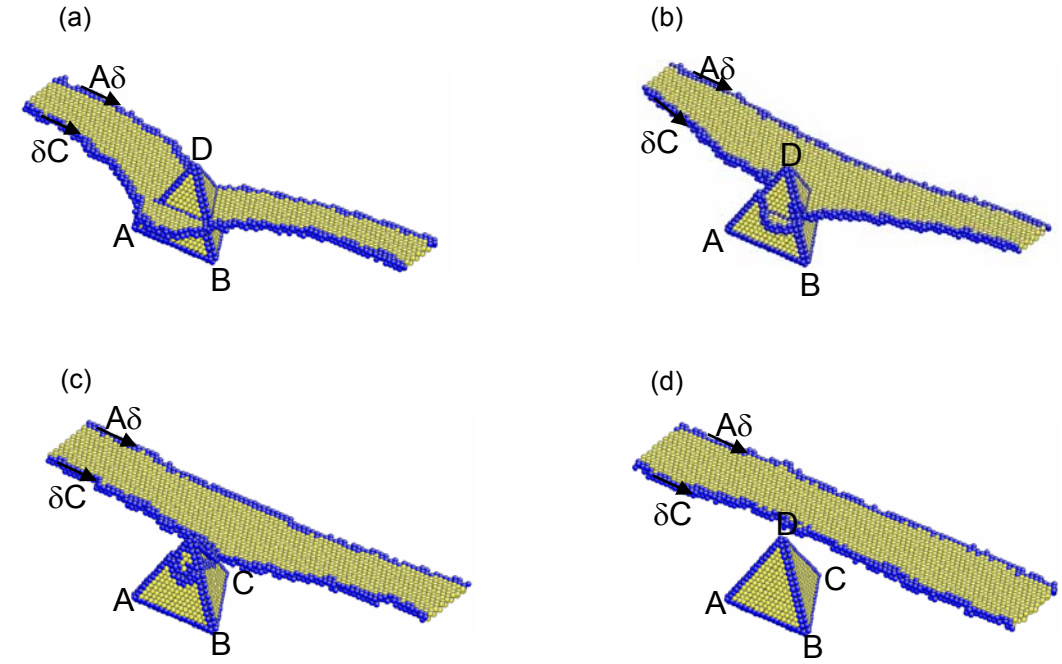

Figure 4. Interaction results of the mixed dislocation, b=AC, intersecting SFT face:

(a) Recombination of the leading partial around the CD edge of the SFT (35ps)
(b) Formation of the I-ledge segment on the c-plane (37ps)
(c) Gliding of shear ledges toward the D apex (38ps)
(d) Complete reconstruction of the SFT (39ps)

Discussions

The partial absorption followed by stable shear ledge of the SFT was observed when b=CA, while a simple dislocation cutting and shear ledge formation that results in complete reconstruction of the SFT was observed in b=AC case. The SFTs with shear ledges (b=CA case) were stable for more than 40 ps at which point, a 2nd dislocation intersection occurs. After the 2nd dislocation intersection, which involved a similar mechanism to the first interaction, the SFT has V- and I- shear ledges, which are sheared by 2b. The effect of applied shear stress (dislocation velocity) was examined by applying a higher shear stress of 300 MPa, but the interaction results were essentially identical. We further analyzed cases that involve (partial) SFT un-faulting (b=CA) as shown below.

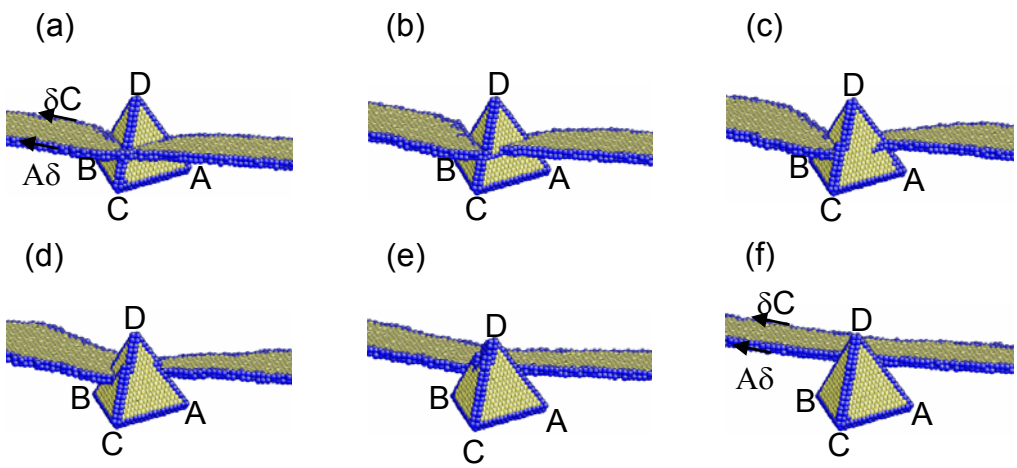

Figure 5. Interaction results of the mixed dislocation, b=AC, intersecting SFT edge:

(a) Intersection on the SFT edge side (36ps)
(b) Constriction on the ACD plane (37ps)
(c) Bypass through the ACD plane (38ps)
(d) I-ledge formation on BCD plane (39ps)
(e) Gliding of shear ledges toward the D apex (40ps)
(f) Complete reconstruction of the SFT (41ps)

<u>Interaction mechanism of dislocation (b=CA) intersecting an SFT edge</u>

The interaction of b=CA intersecting an SFT edge initially shows an un-faulting of the c-plane (Figure 3(c)), which later reconstructed by the dislocation reaction associated with detachment of the leading partial via recombination around the SFT. However, when recombination does not occur, the un-faulting of the c-plane continues and ultimately leads to the absorption of the SFT base. This absorption of the SFT base was observed when the thickness of the simulation cell (x-direction) is reduced to 12.5 nm (20 unit cells). In this case, the same shear stress (100 MPa) was applied to the system but the dislocation velocity was about 2.5 times larger than with the larger cell. Increasing the dislocation velocity at a constant thickness generally produces a larger local bowing of the dislocation around the obstacle. However, in this case, there appears to be less curvature of the dislocation in the thinner sample, which prohibits the subsequent recombination of the leading partial around the SFT. Osetsky and co-workers also report that decreasing the simulation cell thickness reduces the screw dislocation line curvature around an obstacle [11]. This interesting observation is in apparent agreement with our results of SFT base absorption (no recombination of the bowing leading partial dislocation) due to reduced dislocation line curvature. As a result, the dislocation detaches from the SFT with a super-jog pair that has a height corresponding to the distance between the dislocation gliding plane and the SFT base plane.

The initial interaction mechanism is identical to that depicted in Fig. 3(a) to (c). When the dissociated δA and Cδ partial dislocations glide on the (d) plane towards the CD edge of the SFT, constriction occurs on the CD edge and the (a) and (b) faces of SFT. Upon constriction, the dislocation has a screw character on the (b) face of the SFT while it has a 60 degree mixed dislocation character on the (a) face of the SFT. Therefore, it is reasonable to assume that the dislocation on the (b) face cross-slips to βA and Cβ partial dislocations ($\delta A + C\delta \rightarrow CA \rightarrow \beta A + C\beta$) while δA and Cδ on the

(c) face becomes δA, αδ, and Cα ($\delta A + C\delta \rightarrow \delta A + \alpha\delta + C\alpha$) based on the previous observations. However, the constriction and cross-slip occurs very quickly. It is difficult to confirm the individual reactions on both (a) and (b) faces of the SFT.

The δA partial dislocation on the (a) face continues to glide on the (d) plane and reacts with the cross-slipped βA dislocation on the (b) face of the SFT, forming a βα stair-rod partial on the ACD face of the SFT. And the Cβ and Cα Shockley partials glide on the (b)- and (a)-plane of the SFT, respectively, toward the base while removing stacking faults and stair-rod edges around the SFT apex C, as shown in Fig. 6(b). The corresponding dislocation representation is shown in Fig. 6(e).

As shown in Fig. 6 (b) and (e), the δA partial is now constricted on the AD and BD edges and the (c) face of the SFT. Due to the applied shear stress, the Cβ intersects the AD edge (γβ) and $C\beta + \beta\gamma \rightarrow C\beta + \beta A + A\gamma$ occurs. The Aγ removes the stacking fault on the (c)-plane of the SFT as shown in Fig. 6(f). As the dislocation moves away from the SFT, three dislocations around the apex B (γA, αγ, and Cα intersect to form the dislocation CA ($C\alpha + \alpha\gamma + \gamma A \rightarrow CA$). Since the dislocation CA cannot dissociate into Shockley partials on the adjacent (a) or (c) planes, it rearranges its configuration to lie on the (b) plane. In the process, some vacancies are emitted as shown in Fig. 6 (d). The original mixed dislocation now glides with a super-jog pair, which lies on the (b) and (d) planes.

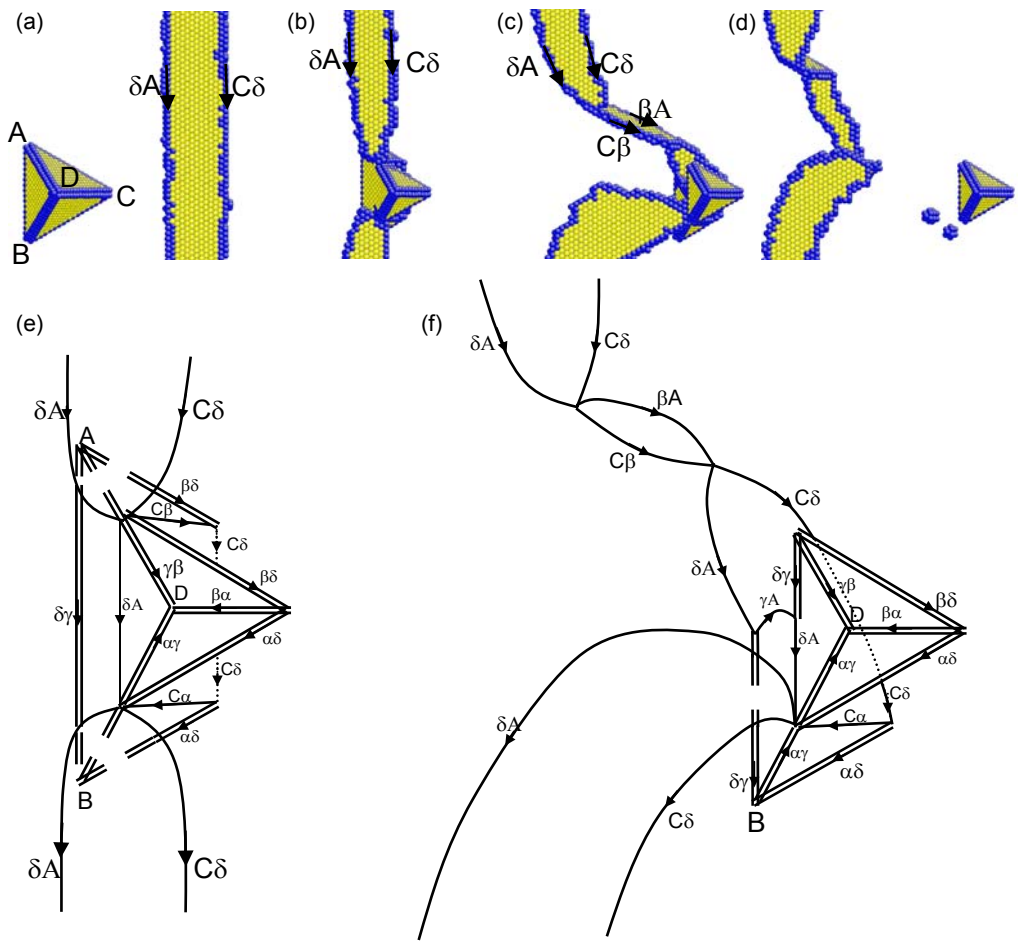

Figure 6. Interaction between a mixed dislocation (b=CA) and an SFT observed in a thinner simulation cell. The MD simulation snapshots are shown in (a)-(d) and the dislocation analysis results are shown in (e) and (f).
(a) Initial configuration. The dislocation glides toward the SFT edge side.
(b) Unfalting of SFT faces.
(c) Super-jog formation.
(d) Final configuration. The smaller SFT and vacancies are left behind.
(e) The dislocation analysis of MD snapshot (b)
(f) The dislocation analysis of MD snapshot (c)

The effect of the applied stress direction

When the shear stress is applied in the y direction (τ_{yx}), the direction of stress is 60 degrees with respect to the direction of the Burgers vector (b=CA). Therefore, the effective stress in the Burgers vector direction is $\tau_{yx}\times\cos(60)$, with an orthogonal component of $\tau_{yx}\times\sin(30)$.

Under this applied stress condition, the interaction between an SFT and a mixed dislocation is different than those previously described. In particular, when the dislocation intersects the SFT face as shown in Fig. 7, the SFT is decomposed into two small perfect SFTs. When the dislocation intersects the SFT edge as shown in Fig. 6, the results are the same as when the applied shear stress is the same direction as the Burgers vector direction.

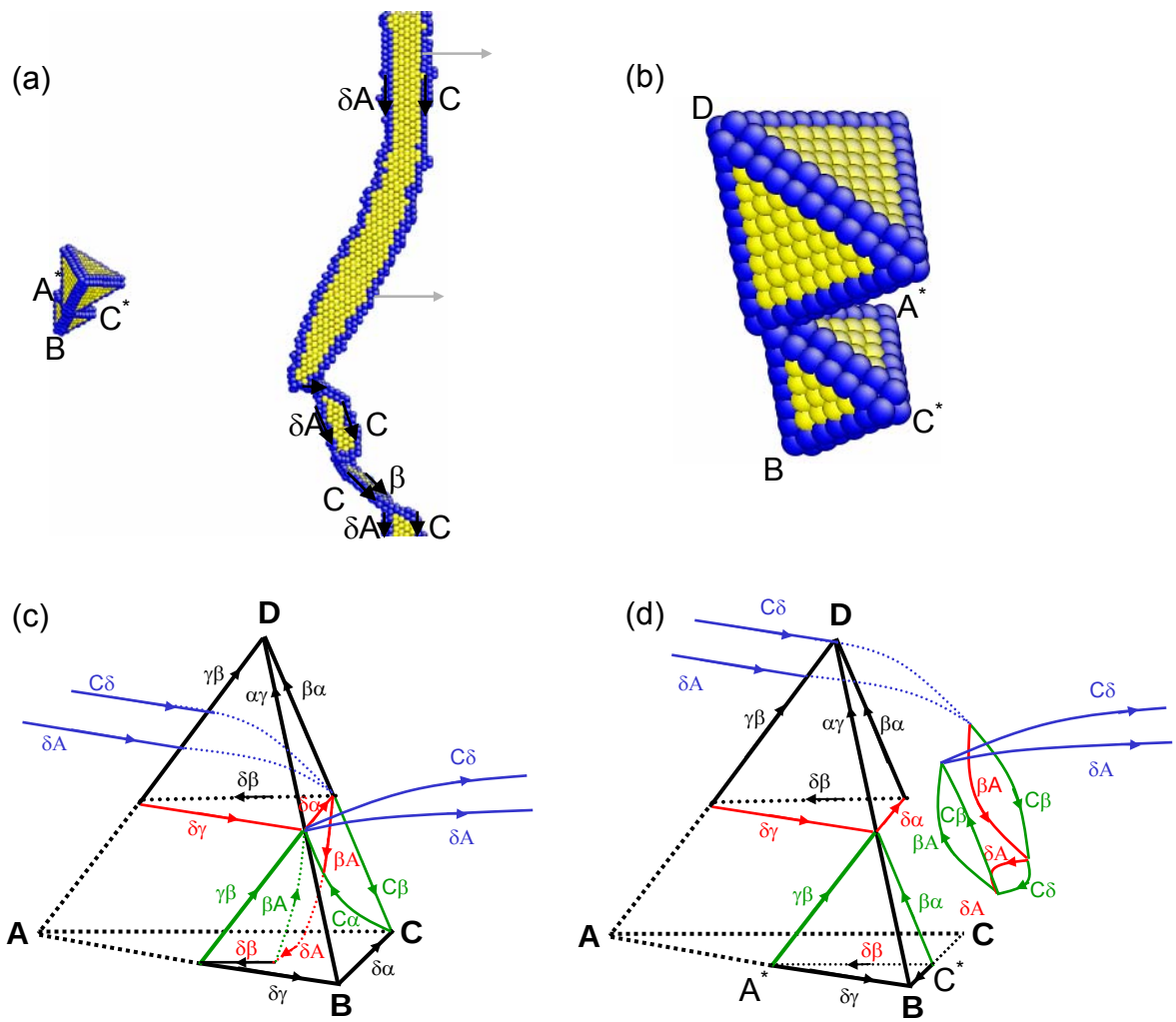

Figure 7. The effect of the applied shear stress direction

Inverse Silcox-Hirsch mechanism

When a mixed dislocation of b=CA glides on the SFT base plane and intersects the SFT face (Fig. 1(a)), the leading Cδ Shockley partial is repelled by the δγ stair-rod dislocation of SFT as shown in Fig. 8(a). This is due to the interaction of two dislocations (Cδ and δγ) that produce a Cγ Frank dislocation upon reaction, which is energetically unfavorable. However, with increasing applied shear stress, the dislocation further glides towards the SFT and the SFT becomes unstable by unzipping from the A apex. The destruction process involves the reverse Silcox-Hirsch mechanism, except the final formation of the Frank loop predicted by Kimura and Maddin is not observed [26], as shown in Figure 8(b)-(d). This behavior is more pronounced for larger SFT, possibly due to the longer edge length of the SFT, and correspondingly longer Cγ Frank partial upon intersection which is energetically less favorable, in addition to the decreased stability of larger SFT with respect to the Frank loop. Thus, complete collapse of the

SFT to a Frank loop by a dislocation may occur for SFT sizes in which the SFT is meta-stable or unstable versus the Frank loop. However, for Cu with a stacking fault energy of 45 mJ/m^2, the size of meta-stable SFTs are about an order of magnitude larger than used in this study. It is also tempting to speculate that this reaction might be responsible for the SFT collapse observed in the in-situ TEM experiments of dislocation interacting with quenched-in SFTs in gold, where the SFTs are of a size corresponding to the meta-stable or unstable size range. In the small (stable) SFTs used in the MD simulations, the partially destructed SFTs reconstructs to a perfect SFT immediately after the dislocation bypass.

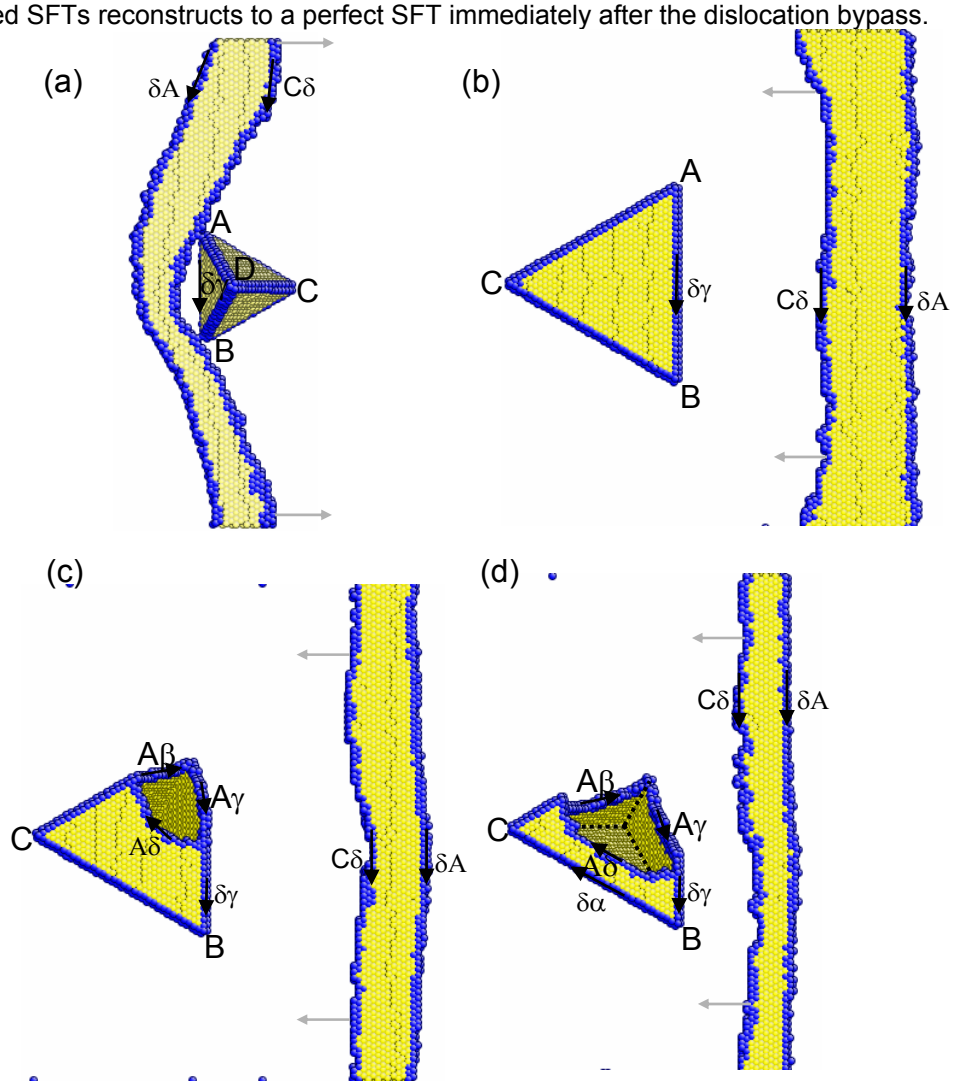

Figure 8. The dislocation gliding on the base plane of the SFT with the interaction geometry of b=CA and SFT face (Fig. 1(a)). The grey arrows indicate the dislocation gliding direction. (a) 4.6 nm size SFT with a projection from the D apex side. (b)-(d) 8.7 nm size SFT with a projection from the SFT base side.

(a) The leading partial (Cδ) is repelled by the AB edge of the SFT (δγ) to avoid the formation of a Frank partial (Cδ+δγ→Cγ).

(b)-(d) The SFT is destructed starting from the A apex of the SFT following the inverse Silcox-Hirsch mechanism.

Conclusions

We have investigated four possible interaction geometries between a 60 degree mixed dislocation and an SFT when the dislocation is gliding about mid-plane between an apex and the SFT base. Depending on the Burgers vector, one case (b=CA) leads to partial absorption, but subsequent stable shear ledge formation is observed on the SFT upon dislocation detachment, while the other case (b=AC) involves simple shear and reconstruction to a perfect SFT. These results were independent of the dislocation intersection geometry, either on the SFT face or the SFT edge.

In case of a dislocation with b=CA, constriction of the mixed dislocation occurs upon contact with the SFT. The trailing Shockley partial cross-slips to glide on the SFT face(s), and leaves a stair-rod partial at the constriction site. When the simulation cell thickness is decreased, absorption of the SFT base into the dislocation core was observed, presumably due to the reduced bowing of the leading partial which limited recombination and detachment around the SFT. The majority of the absorbed vacancies appear as a super-jog pair on the dislocation line, while a couple of vacancies are emitted from the super-jog during the subsequent dislocation glide. In case of b=AC, the individual partials of the dissociated mixed dislocation bypass the SFT separately without constriction. As the trailing partial dislocation detaches from the SFT, the SFT is reconstructed to a perfect SFT by shear ledge glide toward an SFT apex.

Acknowledgements

We gratefully acknowledge the financial support of the Office of Fusion Energy Sciences, U.S. Department of Energy, under Grant DE-FG02-04ER54750, and the DOE-Nuclear Engineering Education Research (NEER) program under Contract No. DE-FG07-04ID14594.

References

[1] B.N. Singh and S.J. Zinkle: Defect accumulation in pure fcc metals in the transient regime: a review. , J. Nuc. Mater. 206, 212 (1993).
[2] T.D. de la RubiA, H.M. Zbib, T.A. Khraishi, et al., Nature 406 (6798): 871-874 (2000)
[3] Ghoniem, N.M., Tong, S.H., Singh, B.N. et al., On dislocation interaction with radiation-induced defect clusters and plastic flow localization in fcc metals. *Philosophical Magazine A - Physics of condensed matter structure defects and mechanical properties* 81 (11), 2743-2764 (2001)
[4] Y. Dai and M. Victoria, Mater. Rex. Soc. Symp. Proc. 439, p319 (1997)
[5] M. Victoria, Journal of Nuclear Materials, 276, 114-122 (2000)
[6] B.L. Eyre and A.F. Bartlett, Philosophical Magazine 12 (116), 261-271 (1965)
[7] B.D. Wirth, V.V. Bulatov, T.D. de la Rubia, Journal of Engineering Materials and Technology, 124, 329 (2002)
[8] Y.N. Osetsky, R.E Stoller, and Y. Matsukawa, Journal of Nuclear Materials, 329-333, 1228 (2004)
[9] Y.N. Osetsky, R.E. Stoller, D. Rodney, D.J. Bacon, Materials Science and Engineering A 400-401, 370 (2005)
[10] D. Rodney, Nuclear Instruments & Methods in Physics Research Section B-Beam Interactions with Materials and Atoms 228, 100-110 (2005)
[11] Y.N. Osetsky, Y. Matsukawa, R.E. Stoller, and S.J. Zinkle, Phil. Mag. Lett. 86 (8), 511 (2006)
[12] Y.N. Osetsky, D. Rodney, D.J. Bacon, Phil. Mag. 86 (16), 2295 (2006)
[13] P. Szelestey, M. Patriarca, and K. Kaski, Modelling Simul. Mater. Sci. Eng. 13, 541 (2005)
[14] H.-J. Lee, J.-H Shim, B.D. Wirth, Journal of Materials Research, 22 (10), (2007)
[15] J.S. Robach, I.M. Robertson, B.D. Wirth, and A. Arsenlis, Phil. Mag. 83 (8), 955 (2003)
[16] Y. Matsukawa, S.J. Zinkle, Journal of Nuclear Materials 329-333: 919-923 Part B AUG 1 (2004)
[17] J.S. Robach, I.M. Robertson, H.-J. Lee, and B.D. Wirth, Acta Mat. 54, 1679 (2006)
[18] Y. Matsukawa, Y.N Osetsky, R.E. Stoller, and S.J. Zinkle, Journal of nuclear materials 351: 285-294 (2006)
[19] H. Kimura, R. Maddin, Lattice defects in quenched metals, in: R. Cotterill (Ed.), Proceedings of an International Conference, Argonne National Laboratory, 15-17 June 1964, Academic Press, New York, p.319 (1965)
[20] I.M. Robertson, personal communication, NEER report (2006)
[21] T.D. de la RUBIA, M.W.GUINAN, Journal of Nuclear Materials 174 (2-3): 151-157 NOV (1990)
[22] Y. Mishin, M.J. Mehl, D.A. Papaconstantopoulos, et al., PHYSICAL REVIEW B 63 (22): Art. No. 224106 JUN 1 (2001)
[23] D. Rodney, *Acta Mater*. 52, 607 (2004)
[24] A.S. Clarke and H. Jonsson, Phys. Rev. E 47, 3975 (1993)
[25] H.J. Lee and B.D. Wirth, Fusion semi-annual report (2005)
[26] J. Silcox J and P.B. Hirsh, Phil. Mag. 4, 72 (1959).